Available online at www.sciencedirect.com

SciVerse ScienceDirect

journal homepage: www.elsevier.com/locate/he

Dehydrogenation mechanisms of $Ca(NH_2BH_3)_2$: The less the charge transfer, the lower the barrier☆

Peng-Fei Yuan [a], Fei Wang [a], Qiang Sun [a], Yu Jia [a,*], Z.X. Guo [b,**]

[a] International Joint Research Laboratory for Quantum Functional Materials of Henan Province, and School of Physics and Engineering, Zhengzhou University, Henan 450001, China

[b] Department of Chemistry, London Center for Nanotechnology, University College London, London WC1H 0AJ, UK

ARTICLE INFO

Article history:
Received 21 May 2013
Received in revised form
19 June 2013
Accepted 24 June 2013
Available online 22 July 2013

Keywords:
Complex hydride
Reaction mechanism
First-principles calculation

ABSTRACT

Our first-principles study of $Ca(NH_2BH_3)_2$ reveals that the gas phase energy barrier for the first H_2 release is 1.90 eV *via* a Ca···H transition state and 1.71 eV *via* an N–H···B transition state for the second H_2 release. In the dimer, the barrier for H_2 release from the bridging $[NH_2BH_3]^-$ species is 1.60 eV *via* an N–H···B transition state, and 0.94 eV *via* an N–H···B transition state for the non-bridging $[NH_2BH_3]^-$ species. Analysis of the atomic charge distribution shows that the mechanism of dehydrogenation is determined by the charge transfer between the transition state and the initial state: the less the charge transfer, the lower the barrier to dehydrogenation.

1. Introduction

One of the most important problems in hydrogen fuel cell technology is the lack of safe and highly efficient hydrogen storage materials [1]. Because of its high storage capacity (19.6 wt%) and moderate dehydrogenation temperature, ammonia borane is considered to be a promising on-board hydrogen storage material [2]. The thermal decomposition of NH_3BH_3 involves three steps evolving one equivalent H_2 per step, at temperatures of ~110, 150, and >500 °C, yielding a final BN product [3–6]. The final step is not considered practical for hydrogen storage because of the very high reaction temperature. However, direct use of NH_3BH_3 is unsuccessful because of borazine formation and the low dehydrogenation kinetics at typical proton exchange membrane fuel cell operating temperatures [2,7,8].

Researchers have attempted to improve the thermal decomposition behavior of solid NH_3BH_3 through a variety of methods, including chemical doping with various transition metals [9,10], base-metal catalysts [11], and acid catalysts [12], as well as particle confinement within nanoscaffolds [7], ionic liquids [13], and carbon cryogels [14]. However, the overall hydrogen storage capacity was reduced by addition of these species, which do not release hydrogen at the operation temperature.

Recently, the substitution of one H(N) [H(N) denotes H bonded to N] atom in the compound by a metal atom has been investigated as a potential route to modify the kinetics and

* *Corresponding author*. Tel.: +86 371 67739336.
** *Corresponding author*. Tel.: +44 (0) 20 76797527.
E-mail addresses: jiayu@zzu.edu.cn (Y. Jia), z.x.guo@ucl.ac.uk (Z.X. Guo).

0360-3199/$ – see front matter
http://dx.doi.org/10.1016/j.ijhydene.2013.06.106

thermodynamics of H_2 release from NH_3BH_3. So far, most of the metal atoms investigated are from the alkali and alkaline-earth groups. Some metal amidoboranes have been synthesized (i.e. $LiNH_2BH_3$ [15–20], $NaNH_2BH_3$ [16,20,21], $Ca(NH_2BH_3)_2$ [18,22,23] and $Sr(NH_2BH_3)_2$ [24]), and show a significant enhancement of dehydrogenation kinetics, along with suppressed borazine release. For example, $LiNH_2BH_3$ releases most of the hydrogen at ~92 and 120 °C; the thermal dehydrogenation of $NaNH_2BH_3$ resembles that of $LiNH_2BH_3$, but at a slightly lower temperature of 89 °C; and $Ca(NH_2BH_3)_2$ releases hydrogen at ~100 and 140 °C [16,18].

To improve the operating properties of these materials, especially rapid H_2 release near room temperature, it is important to understand the underlying mechanism for the release of H_2 from these compounds. Previous theoretical studies have focused on NH_3BH_3 and $LiNH_2BH_3$ [25–33], and have indicated that H_2 is released *via* an N–H···B transition state in NH_3BH_3 and a Li···H transition state in $LiNH_2BH_3$ in the gas phase. For the dimer case, the mechanism is more complex. The energy barriers for H_2 release were also calculated. The overall results agree well with the variation of the dehydrogenation temperature [18]. For example, Shevlin et al. performed a detailed study on isolated NH_3BH_3, $LiNH_2BH_3$, and their dimers [33]. In the gas phase, the energy barrier is 1.39 eV for the first H_2 release from an NH_3BH_3 molecule *via* an N–H···B transition state. For $LiNH_2BH_3$, the barrier is 1.61 eV and the metal moiety acts as a hydrogen shuttle in a two-stage dehydrogenation mechanism. For the dimers, the energy barriers are 1.22 eV for NH_3BH_3 and 0.71 eV for $LiNH_2BH_3$, which helps to explain the observed experimental dehydrogenation temperatures of 92 °C for $LiNH_2BH_3$ and 110 °C for NH_3BH_3. Recently, a systematic study of the dehydrogenation mechanisms of Group I and Group II metal amidoboranes was performed by Kim et al. [34]. In their study, in which not only the M···H transition state but also the oligomerization transition state were considered, they found that the metal cation plays a role as a hydride-transfer catalyst.

Though the dehydrogenation mechanism of $LiNH_2BH_3$ has been well explained, a detailed study of other metal amidoboranes is still lacking, especially for $Ca(NH_2BH_3)_2$, the alkaline-earth metal amidoborane. Additionally, the dehydrogenation of $Ca(NH_2BH_3)_2$ is endothermic, whereas it is exothermic for all the other metal amidoboranes. This atypical behavior may be caused by a unique dehydrogenation mechanism. Therefore, we have performed a comprehensive study of $Ca(NH_2BH_3)_2$ dehydrogenation mechanism based on density functional theory.

2. Computational methods

First-principles calculations were carried out within the density functional theory framework [35]. We used the projector-augmented wave (PAW) method [36,37] and the generalized gradient approximation (GGA) [38] for the exchange-correlation energy functional, as implemented in the Vienna *ab initio* simulation package (VASP) [39–41]. The GGA calculation was performed with the Perdew–Burke–Ernzerhof (PBE) [42] exchange-correlation potential. First, the crystal structure was optimized. $Ca(NH_2BH_3)_2$ has a monoclinic structure with the C2 space group. The unit cell contains 30 atoms [18]. The equilibrium lattice parameters were calculated using a plane-wave cutoff energy of 400 eV and a $3 \times 3 \times 3$ k-point mesh within the Monkhorst–Pack [43] scheme. In the calculation, self-consistency was achieved with a tolerance in total energy of 0.01 meV, and when the forces on each atom were less than 0.01 eV/Å. The optimized lattice parameters were found to be $a = 9.254$ Å, $b = 4.496$ Å, $c = 6.599$Å, and $\beta = 91.26°$. This result is in good agreement with the experimentally determined parameters: $a = 9.100$ Å, $b = 4.371$ Å, $c = 6.441$ Å, and $\beta = 93.19°$ [18]. Subsequent calculations were performed with the same optimized lattice parameters. Simulation cells of size $15 \times 15 \times 15$ Å^3 were used for the isolated molecule and $20 \times 20 \times 20$ Å^3 for the dimers. The Nudged Elastic Band (NEB) method [44] was used to determine the minimum energy pathway. All atoms were fully relaxed with tolerances in total energy of 0.01 meV, and for the forces on each atom of 0.01 eV/Å.

3. Results and discussion

3.1. Dehydrogenation mechanism in the gas phase

To understand the dehydrogenation mechanism of $Ca(NH_2BH_3)_2$, we first studied the basic properties of the compound in the gas phase. The molecular structure is shown in Fig. 1(a), and the bond lengths and bond angles are listed in Table 1. The calculated N–B bond length is 1.58 Å, which is shorter than that of crystalline (bulk) NH_3BH_3, but similar to that in $LiNH_2BH_3$ and $NaNH_2BH_3$. The N–H bond length is 1.02 Å and the B–H bond lengths are 1.21, 1.26, and 1.26 Å. The N–H bond length is similar to that in NH_3BH_3, $LiNH_2BH_3$, and $NaNH_2BH_3$, but the B–H bond lengths are slightly longer than those in NH_3BH_3. This means that the identity of the metal atom has little effect on the $[NH_2BH_3]^-$ structure. Furthermore, this structure also shows negligible deviation from the crystal phase. The Ca atom resides in a bridge over the B–N bond, with a Ca–N distance of 2.32 Å and a Ca–N–B angle of 76.0°. The Ca atom coordinates with four H(B) [H(B) denotes H bonded to B] atoms with a Ca–H(B) distance in the range of 2.30–2.33 Å. This is different from that in the crystal phase, where the Ca–N distance is 2.48 Å, the Ca–H(B) distance is in the range of 2.36–2.41 Å, and the Ca–N–B angle is 113.2°. In both phases, the Ca–H(N) distance is longer than 3.0 Å. Previous studies have shown that the $H^+\cdots H^-$ interaction plays an important role in hydrogen storage [45]. In the gas phase, the shortest $H^+\cdots H^-$ distance that appears in either $[NH_2BH_3]^-$ group was about 2.56 Å, which is longer than the maximum dihydrogen bond length (2.4 Å). Additionally, the calculated N–B bond cleavage energy is 2.82 eV, which is smaller than that of $LiNH_2BH_3$ and $NaNH_2BH_3$, but larger than that of NH_3BH_3 [33], which is consistent with the electronegativity ordering of the substituents.

Mechanistically, previous studies show that while H_2 is released through an N–H···B transition state for NH_3BH_3, dehydrogenation proceeds *via* an M···H transition state for MNH_2BH_3 (M = Li, Na) [25–33]. We calculated the energy barrier of both processes for $Ca(NH_2BH_3)_2$. The calculated results are shown in Fig. 2 and the molecular structures of the

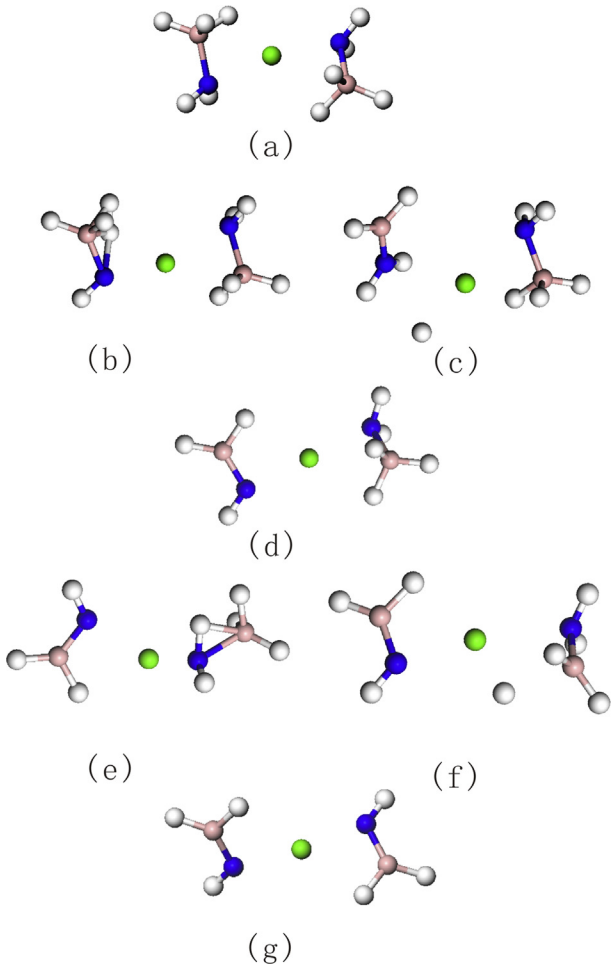

Fig. 1 – Relaxed molecular structures of $Ca(NH_2BH_3)_2$: (a) initial state, (b) transition state TS1a, (c) transition state TS1b, (d) final state FS1, (e) transition state TS2a, (f) transition state TS2b, (g) final state FS2. Green, pink, blue, and white spheres denote Ca, B, N, and H atoms, respectively. (For interpretation of the references to color in this figure legend, the reader is referred to the web version of this article.)

transition states and the final state (**FS1**) are shown in Fig. 1(b)–(d) (Fig. 1(a) is the initial state (**IS1**)). For dehydrogenation, the system needs to overcome energetic barriers of 2.70 and 1.90 eV to pass through the N–H···B (**TS1a**) and the Ca···H (**TS1b**) transition states, respectively. Therefore, **TS1b** is the most likely mechanism, which is similar to that in $LiNH_2BH_3$ (a barrier of 1.61 eV is encountered in $LiNH_2BH_3$). In both processes, only one $[NH_2BH_3]^-$ releases H_2, without evident interaction with the other. A discussion of the structural change in the reacted $[NH_2BH_3]^-$ follows. The calculated bond lengths and bond angles of **TS1a**, **TS1b**, and **FS1** are also listed in Table 1. It is noted that in **TS1a**, one of the N–H bond lengths changes from 1.02 to 1.52 Å, and that this H(N) atom also coordinates with the B atom, with a B–H(N) bond length of 1.46 Å, and with the Ca atom, with a Ca–H(N) distance of 2.87 Å. One B–H(B) bond length also changes from 1.26 to 1.37 Å. The length between these two H atoms [H(N) and H(B)] is 0.97 Å. These changes make the Ca–H(B) distances longer than that in **IS1**. The Ca–N–B angle also increased. In **TS1b**, the largest change is the N–B bond length, from 1.58 to 1.40 Å, which is indicative of double bond formation; this is similar to that seen in **FS1**, where the $[NHBH_2]^-$ is a planar structure. The Ca–N distance and Ca–H(B) distance are also longer than that in **IS1**. The distance between Ca and the released H(B) atom is 2.07 Å.

To further understand the mechanisms, we used Bader charge analysis [46] to monitor changes in the charges on each atom in both processes, including the initial state, the transition states, and the final state. The calculated results are listed in Table 2. It is clear that the charge transferred between the transition states and the initial state is different. In **TS1a**, one H(N) atom gains 0.21e and the N atom gains 0.18e, while two H(B) atoms lose 0.05e and 0.29e and the B atom loses 0.06e; the overall total charge transfer is 0.39e and occurs among different types of atoms. In **TS1b**, one H(B) atom receives 0.15e and the N atom receives 0.14e, while two H(N) atoms lose 0.07e and 0.10e and the B atom loses 0.13e. In this case, the total overall charge transfer, which also occurs among different types of atoms, is only 0.29e. Therefore, the results indicate that the less the charge transfer, the lower the barrier to dehydrogenation of the compound.

Next, the barrier for the second H_2 release was studied. First, we determine from which group the H_2 will be released, $[NH_2BH_3]^-$ or $[NHBH_2]^-$. The calculated results show that H_2 release from $[NH_2BH_3]^-$ is energetically favorable and is 0.74 eV lower than release from $[NHBH_2]^-$. In other words, after the second H_2 is released, the $Ca(NHBH_2)_2$ molecule will be formed. As for the first H_2 release, the two different dehydrogenation mechanisms were considered. The calculated barriers are shown in Fig. 1, and the molecular structures of the transition states and final states (**FS2**) are shown in Fig. 1(e)–(f). Interestingly, the energy barriers are 1.71 eV and 2.21 eV for the N–H···B (**TS2a**) and the Ca···H (**TS2b**) transition states, respectively. This ordering is different than for the first dehydrogenation step (release of the first H_2). In both processes, the resulting $[NHBH_2]^-$ shows negligible geometric changes. The structural changes in the $[NH_2BH_3]^-$ molecule as it reaches the transition state are discussed as follows. The calculated bond lengths and bond angles of all the transition states and final state are listed in Table 1. From this table, we can see that in **TS2a**, one N–H bond length changes from 1.02 to 1.07 Å, and this H(N) atom also coordinates with the B atom, with a B–H(N) bond length 1.52 Å, and the Ca atom, with a Ca–H(N) distance of 2.66 Å. The B–H(B) bond lengths undergo very small changes (<0.02 Å). The N–B bond elongates, from 1.58 to 1.65 Å. The $H(N)^+\cdots H(B)^-$ distance is 1.45 Å. The Ca–H(B) distances also change, with one extending from 2.32 to 2.77 Å, and the other to longer than 3.0 Å. The Ca–N–B angle also increases. In **TS2b**, the structural changes are predominately seen in the N–B bond length, which decreases from 1.58 to 1.46 Å, and the Ca–N distance, increasing from 2.36 to 2.50 Å. The distance between Ca and the released H(B) atom is 2.03 Å.

In the first dehydrogenation step, we found that the less the charge transfer, the lower the barrier to dehydrogenation of the compound. To ascertain the generality of this observation, we investigate whether this trend holds for the second

Table 1 – Calculated B–N, B–H, and N–H bond lengths (A) and the Ca–N and Ca–H(B) distances for the initial state, transition states, and final states of $Ca(NH_2BH_3)_2$ monomer at different H_2 releasing steps. The calculated Ca–N–B bond angles (deg.) are also presented. The values for the crystal phase (Cry) are listed for comparison.

	Step1				Step 2				Cry
	IS1	TS1a	TS1b	FS1	IS2	TS2a	TS2b	FS2	
Bond length (Å)									
B–N	1.58	1.53	1.40	1.38	1.58	1.65	1.46	1.38	1.55
B–H	1.21	1.21	1.20	1.21	1.22	1.21	1.20	1.20	1.23
	1.26	1.26	1.21	1.26	1.25	1.25	1.24	1.26	1.24
	1.26	1.37			1.25	1.27			1.25
		1.46				1.52			
N–H	1.02	1.02	1.02	1.02	1.02	1.02	1.02	1.02	1.02
		1.52				1.07			
Ca–N	2.32	2.20	2.79	2.21	2.36	2.20	2.21	2.22	2.48
		2.38	2.50	2.35		2.18	2.72		
Ca–H(B)	2.30	2.37	2.25	2.31	2.31	2.26	2.27	2.30	2.36
	2.33	2.58	2.28	2.32	2.32	2.77	2.50	2.32	2.37
		2.26		2.36	2.36				2.41
		2.29							
Bond angle (deg.)									
Ca–N–B	76.0	88.2	87.0	93.7	76.0	92.5	92.0	92.8	113.2
		73.9	71.4	76.2		107.5	74.4	93.0	

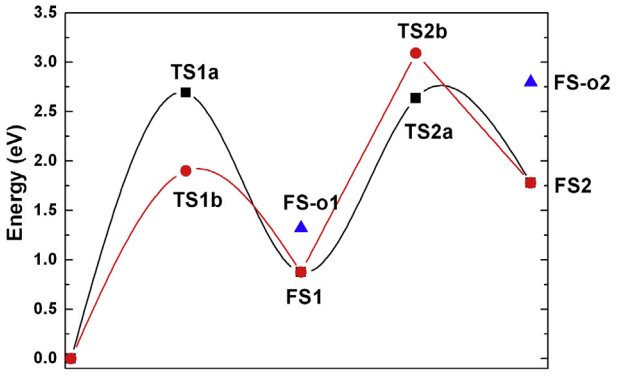

Fig. 2 – Schematic electronic energy profiles for the first and second H_2 release from $Ca(NH_2BH_3)_2$, *via* different transition states. FS-o1 and FS-o2 are the energy for the oligomerization process. The energy of $Ca(NH_2BH_3)_2$ has been set to zero. Lines are drawn to guide the eye.

H_2 release step. The calculated charges on each atom in both processes are listed in Table 2. From the data, we compute a total charge transfer of 0.11e for **TS2a** and 0.24e for **TS2b**. Once again, we found that the less the charge transfer, the lower the barrier. In a previous study, Kim et al. also calculated the energy barrier *via* the Ca···H transition state [34]. Their results indicate barriers of 1.55 eV for the first H_2 release, and 2.04 eV for the second H_2 release. Our results (1.90 eV for the first and 2.21 eV for the second) are in good agreement with theirs, but the N–H···B process is not included in their studies. They also calculated the energy barrier of the oligomerization process, and the barrier is 1.86 eV for the first and the second H_2 release. The energy of both final states is higher than that of the non-oligomerization process. We also considered this process, and arrive at similar results, but with a higher barrier.

Additionally, the barrier for release of the third and fourth H_2 was calculated. For the third H_2 release, the calculated energy barriers *via* the N–H···B and the Ca···H process are equal, about 3.34 eV, and the charge transfer is also equal, about 0.55e. This result also fits with the aforementioned trend: the less the charge transfer, the lower the barrier. For

Table 2 – Calculated Bader charges (with respect to neutral atom) for the initial state, transition states, and final states of $Ca(NH_2BH_3)_2$ monomer at different H_2 releasing steps. The values for the crystal phase (Cry) are also listed for comparison.

	Step 1				Step2				Cry
	IS1	TS1a	TS1b	FS1	IS2	TS2a	TS2b	FS2	
Ca	+1.528	+1.527	+1.524	+1.542	+1.550	+1.533	+1.489	+1.545	+1.557
B	+1.702	+1.764	+1.834	+1.807	+1.693	+1.677	+1.817	+1.803	+1.719
N	−1.500	−1.678	−1.638	−1.818	−1.510	−1.599	−1.665	−1.754	−1.592
H(B)	−0.575	−0.526	−0.573	−0.585	−0.565	−0.574	−0.575	−0.576	−0.613
	−0.606	−0.605	−0.754	−0.645	−0.599	−0.615	−0.638	−0.642	−0.600
	−0.593	−0.300	−0.579		−0.598	−0.567	−0.574		−0.582
H(N)	+0.406	+0.398	+0.495	+0.472	+0.419	+0.431	+0.444	+0.398	+0.432
	+0.401	+0.189	+0.473		+0.387	+0.458	+0.471		+0.460

the fourth H_2 release, we could only successfully obtain a single barrier of about 3.09 eV. The related structural information and the calculated atom charges can be seen in the Supporting information (Fig. S1, Tables S1 and S2).

Overall, we found that if there is more than one pathway to reach the final state, the energy barrier of each process is determined by the charge transfer between the transition state and the initial state: the less the charge transfer, the lower the barrier.

3.2. *Dehydrogenation mechanism in the dimer*

In practice, dehydrogenation often occurs in the solid phase. Therefore, it is important to study the effect of neighboring molecules on the dehydrogenation mechanism. Here, the dimer was studied. The optimized structure is shown in Fig. 3(a) and the calculated bond lengths and bond angles are listed in Table 3. The four $[NH_2BH_3]^-$ groups can be separated into two types: one (the non-bridging one) associated with one Ca atom, the other (the bridging one) with two Ca atoms. Here, each Ca atom is coordinated with three $[NH_2BH_3]^-$ groups through two Ca–N interactions, with distances of 2.37 Å (non-bridging), 2.40 Å (bridging), 2.36 Å (non-bridging), and 2.48 Å (bridging); and one Ca–B interaction with distances of 2.70 Å (bridging) and 2.87 Å (bridging). This structure is still different from that in the crystal phase, where each Ca directly coordinates with two $[NH_2BH_3]^-$ groups with a closest Ca–N distance of ~2.50 Å, and the other four $[NH_2BH_3]^-$ groups with Ca–B distances in the range of 2.90–3.16 Å, forming an octahedron. Both the N–H and the B–H bond lengths are unchanged when compared with those in the monomer (our results in Table 1). However, the four N–B bond lengths changed from 1.55 to 1.58 Å. The shortest one is the same as that in the solid phase and the longest one is the same as that in the gas phase. Further analysis shows that the shorter two belong to the bridging $[NH_2BH_3]^-$, and the longer two belong to the non-bridging $[NH_2BH_3]^-$. As they have slightly different geometries, H_2 release from different $[NH_2BH_3]^-$ groups may proceed through different energy barriers. The shortest $H^+\cdots H^-$ distance of 2.45 Å is still found within one $[NH_2BH_3]^-$ moiety (non-bridging), while the distance in the bridging species is 2.60 Å, and the distance between two nearby bridging $[NH_2BH_3]^-$ groups is 2.65 Å. The above analysis indicates that H_2 may release through three different pathways: from the non-bridging $[NH_2BH_3]^-$, from the bridging $[NH_2BH_3]^-$, or from two nearby bridging $[NH_2BH_3]^-$ (oligomerization process). The energy barriers of the two non-oligomerization processes were studied first. Also, two different dehydrogenation mechanisms were considered. The calculated energy barrier is shown in Fig. 4. The structures of all the transition states and final states are shown in Fig. 3(b)–(g). Here, we can see that the energy barriers for **FSd1** (the final state when H_2 is released from the bridging $[NH_2BH_3]^-$) are 1.60 eV and 4.28 eV for the N–H···B (**TSd1a**) and Ca···H (**TSd1b**) transition states; for **FSd2** (the final state when H_2 is released from the non-bridging $[NH_2BH_3]^-$), the energy barriers are 0.94 eV and 1.90 eV for the N–H···B (**TSd2a**) and the Ca···H (**TSd2b**) transition states. The total energy of **FSd2** is 0.38 eV lower than that of **FSd1**.

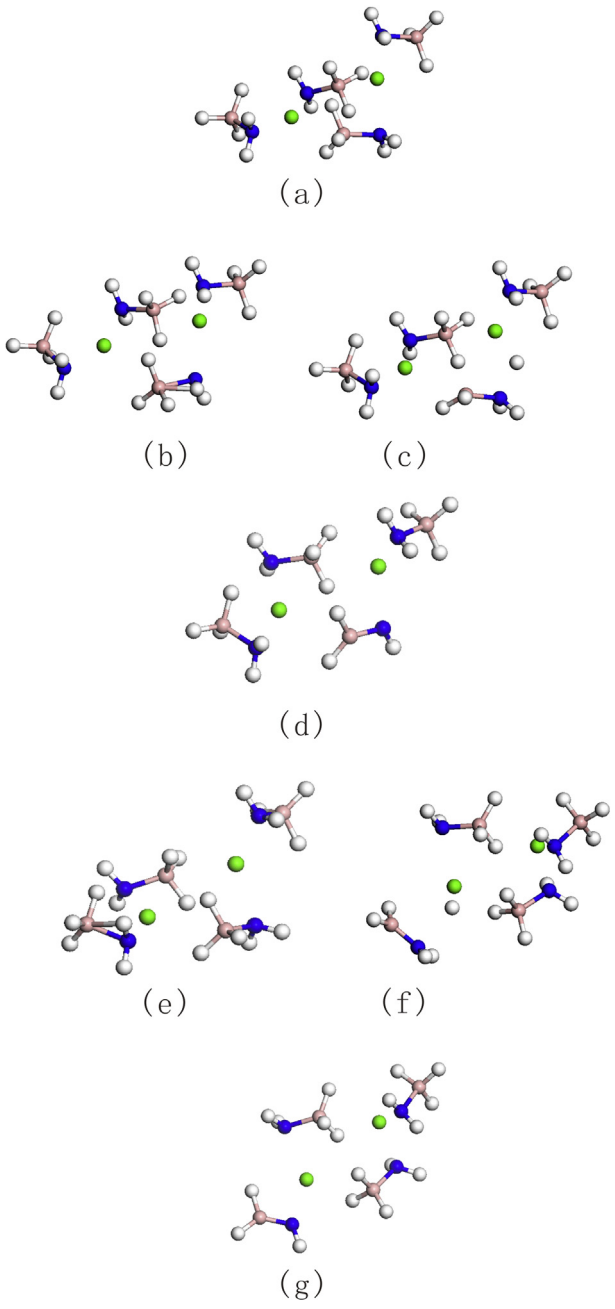

Fig. 3 – Relaxed molecular structures of the $Ca(NH_2BH_3)_2$ dimer: (a) initial state, (b) transition state TSd1a, (c) transition state TSd1b, (d) final state FSd1, (e) transition state TSd2a, (f) transition state TSd2b, (g) final state FSd2. Green, pink, blue, and white spheres denote Ca, B, N, and H atoms, respectively. (For interpretation of the references to color in this figure legend, the reader is referred to the web version of this article.)

Then, the structural changes are explored. The calculated bond lengths and bond angles are listed in Table 3. In **TSd1a**, one N–H bond length changes from 1.02 to 1.05 Å, and this H(N) atom also coordinates with the B atom, with a B–H(N) bond length of 1.58 Å. The B–N bond length changes from 1.56 to 1.63 Å, and the Ca–H(B) distance changes substantially,

Table 3 – Calculated B–N, B–H, and N–H bond lengths (A) and the Ca–N and Ca–H(B) distances for the initial state, transition states, and final states of the $Ca(NH_2BH_3)_2$ dimer. The calculated Ca–N–B bond angles (deg.) are also presented. Only the reacted $[NH_2BH_3]^-$ group is listed.

	Bridging				Non-bridging			
	ISd	**TSd1a**	**TSd1b**	**FSd1**	**ISd**	**TSd2a**	**TSd2b**	**FSd2**
Bond length (Å)								
B–N	1.56	1.63	1.52	1.34	1.57	1.60	1.40	1.38
B–H	1.21	1.23	1.21	1.22	1.22	1.22	1.21	1.21
	1.24	1.25	1.23	1.25	1.26	1.23	1.20	1.25
	1.29	1.33			1.26	1.26		
		1.58				1.68		
N–H	1.02	1.02	1.02	1.02	1.02	1.03	1.02	1.02
		1.05	1.03			1.03		
Ca–N	2.40	2.38	2.72	2.32	2.36	2.25	2.82	2.21
Ca–H(B)	2.30	2.97	2.25	2.34	2.35	2.43	2.98	2.41
	2.35	2.97		2.67	2.36			
	2.32	2.86		2.55				
Bond angle (deg.)								
Ca–N–B	90.0	107.4	85.0	95.8	76.8	91.2	89.8	92.0

from about 2.3 Å to nearly 3.0 Å. In **TSd1b**, the biggest change is seen in the Ca–N distance, which increases from 2.40 to 2.72 Å. The number of Ca–H(B) interactions decreases from three to one. In **TSd2a**, the changes are very small. In **TSd2b**, the B–N bond length changes from 1.57 to 1.40 Å, and the Ca–N distance changes from 2.36 to 2.82 Å. The number of Ca–H(B) interactions also decreases, from two to one (this remaining interaction has a distance of 2.98 Å, and is then very weak). In all four states, the un-reacted $[NH_2BH_3]^-$ groups show negligible changes, and the overall structure also has very small changes. From the above analysis, we can see that all the four transition states in the dimer cases have tendencies similar to that in the gas phase, with the same dehydrogenation mechanism. The $H^+\cdots H^-$ distance is 1.51 Å in **TSd1a** and 1.80 Å in **TSd2a**, and the distance between Ca and the released H(B) atom is 2.14 Å in **TSd1b** and 2.03 Å in **TSd2b**.

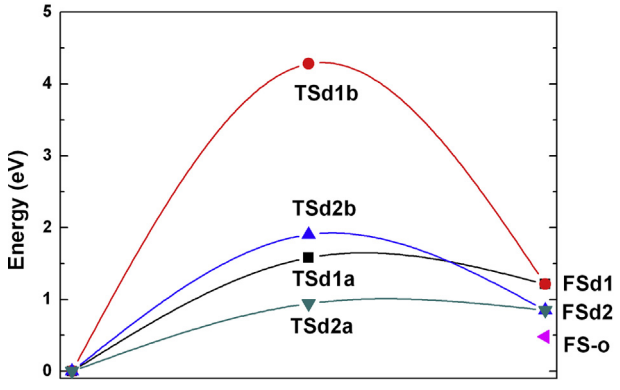

Fig. 4 – Schematic electronic energy profiles for H_2 release from $Ca(NH_2BH_3)_2$ dimer to two different final states (FSd1 and FSd2), each *via* two different transition states (TSd1a, TSd1b and TSd2a, TSd2b). FS-o is the energy for the oligomerization process. The energy of the $Ca(NH_2BH_3)_2$ dimer has been set to zero. Lines are drawn to guide the eye.

From the gas phase, we observed that a lower barrier may be caused by less charge transfer. Therefore, we also calculated the charges on each atom for all four processes, the results of which are listed in Table 4. The charge transfer was found to be 0.10e, 0.14e, 0.58e, and 0.19e for the **TSd1a**, **TSd2a**, **TSd1b**, and **TSd2b** transition states, respectively. Barrier calculation also shows that both **TSd1a** and **TSd2b** involve a lower energy barrier than that of the other processes. Thus, the same observation applies to the dimer case: the less the charge transfer, the lower the barrier to dehydrogenation.

Next, the oligomerization process was studied. As we have discussed earlier, this process may happen between two bridging $[NH_2BH_3]^-$ species, and the $H^+\cdots H^-$ distance is 2.65 Å, which is longer than the 2.4 Å van der Waals distance for the interaction constituting a dihydrogen bond. First, the structure after H_2 release was optimized. The calculated total energy is 0.37 eV lower than that of **FSd2**. This indicated that oligomerization is energetically more favorable than the non-oligomerization process. Calculation of the energy barrier is then needed to determine whether this process is kinetically favorable. Unfortunately, direct barrier calculation was unsuccessful, so we chose another method to test whether the final state could be formed. In previous studies of $Mg(BH_4)_2{\cdot}2NH_3$ and $Ca(NH_2BH_3)_2{\cdot}2NH_3$, one H(B) atom was removed from the compound and the structure was optimized. Then, an H(N) atom was removed from the optimized structure, and the resulting structure was also optimized [47,48]. The final optimized structure was used to study the initial dehydrogenation mechanism. By this method, the authors were able to successfully demonstrate the formation of an N–B bond after dehydrogenation. These studies encouraged us to use this method to search for the formation of an N–B bond in the dimer, but we did not observe N–B bond formation. This could indicate that the oligomerization process may not be feasible for a dimer system. A possible reason may be the longer $H^+\cdots H^-$ distance. Experimentally, researchers have observed the existence of N–B–N structures [22]. A previous theoretical study has also shown that for $M{-}NH_2BH_3$, the calculated reaction enthalpy is closer to the

Table 4 – Calculated Bader charges (with respect to neutral atom) for the initial state, transition states, and final states of the $Ca(NH_2BH_3)_2$ dimer. Only the reacted $[NH_2BH_3]^-$ group is listed.

	Bridging				Non-bridging			
	ISd	TSd1a	TSd1b	FSd1	ISd	TSd2a	TSd2b	FSd2
Ca	+1.528	+1.561	+1.468	+1.538	+1.542	+1.523	+1.471	+1.536
B	+1.713	+1.658	+1.260	+1.773	+1.683	+1.668	+1.827	+1.775
N	−1.585	−1.625	−1.543	−1.730	−1.614	−1.662	−1.615	−1.793
H(B)	−0.619	−0.621	−0.073	−0.647	−0.592	−0.600	−0.696	−0.636
	−0.607	−0.609	−0.645	−0.607	−0.595	−0.592	−0.597	−0.585
	−0.557	−0.519	−0.568		−0.569	−0.551	−0.564	
H(N)	+0.449	+0.470	+0.494	+0.430	+0.467	+0.518	+0.495	+0.472
	+0.434	+0.425	+0.401		+0.452	+0.453	+0.458	

experimental value if the final product is M–$NHBHNHBH_3$ [49]. The oligomerization process may happen in $Ca(NH_2BH_3)_2$ trimers or larger clusters, and this will be interesting for further study.

4. Conclusions

In summary, the dehydrogenation mechanism of $Ca(NH_2BH_3)_2$ was elucidated by first-principles density functional methods. In the gas phase, the barrier for the first H_2 release is 1.90 eV *via* the Ca···H transition state and 2.70 eV *via* the N–H···B transition state; the barrier for the second H_2 release is 2.21 eV *via* the Ca···H transition state and 1.71 eV *via* the N–H···B transition state. For the dimer, the barrier for H_2 release from the bridging $[NH_2BH_3]^-$ species is 4.28 eV *via* the Ca···H transition state and 1.60 eV *via* the N–H···B transition state, while the barrier for H_2 release from the non-bridging $[NH_2BH_3]^-$ species is 1.90 eV *via* the Ca···H transition state and 0.94 eV *via* the N–H···B transition state. The oligomerization process in the gas phase and the dimer were also calculated, and both are kinetically unfavorable. Charge analysis shows that the process with a lower barrier corresponds to that with less charge transfer. Hence the dehydrogenation mechanism is driven by charge transfer between the transition state and the initial state: the less the charge transfer, the lower the barrier.

Acknowledgments

The work was supported partly by the "973 Project" (No. 2012CB921300), partly by the NSF of China (Grant No. 11274280), and partly by the Program for Innovative Research Team of Science and Technology of Henan Province (Grant No: 2012IRTSTHN003). ZXG is supported by the UK EPSRC through the SUPERGEN Initiative (EP/E040071/1, EP/E046193/1, EP/K002252/1). The calculations were performed on the High Performance Clusters of Zhengzhou University.

Appendix A. Supplementary data

Supplementary data related to this article can be found at http://dx.doi.org/10.1016/j.ijhydene.2013.06.106.

REFERENCES

[1] Graetz J. New approaches to hydrogen storage. Chem Soc Rev 2009;38:73–82.
[2] Stephens FH, Pons V, Tom Baker R. Ammonia–borane: the hydrogen source par excellence. Dalton Trans 2007;25:2613–26.
[3] Sit V, Geanangel RA, Wendlandt WW. The thermal dissociation of NH_3BH_3. Thermochim Acta 1987;113:379–82.
[4] Hu MG, Geanangel RA, Wendlandt WW. The thermal decomposition of ammonia borane. Thermochim Acta 1978;23:249–55.
[5] Wolf G, Baumann J, Baitalow F, Hoffman P. Calorimetric process monitoring of thermal decomposition of B–N–H compounds. Thermochim Acta 2000;343:19–25.
[6] Baitalow F, Baumann J, Wolf G, Jaenicke-Rößler K, Leitner G. Thermal decomposition of B–N–H compounds investigated by using combined thermoanalytical methods. Thermochim Acta 2002;391:159–68.
[7] Gutowska A, Li L, Shin Y, Wang CM, Li XS, Linehan JC, et al. Nanoscaffold mediates hydrogen release and the reactivity of ammonia borane. Angew Chem Int Ed 2005;44:3578–82.
[8] Marder TB. Will we soon be fueling our automobiles with ammonia–borane. Angew Chem Int Ed 2007;46:8116–8.
[9] Jaska CA, Temple K, Lough AJ, Manners I. Transition metal-catalyzed formation of boron–nitrogen bonds: catalytic dehydrocoupling of amine–borane adducts to form aminoboranes and borazines. J Am Chem Soc 2003;125:9424–34.
[10] Denney MC, Pons V, Hebden TJ, Heinekey M, Goldberg KI. Efficient catalysis of ammonia borane dehydrogenation. J Am Chem Soc 2006;128:12048–9.
[11] Keaton RJ, Blacquiere JM, Baker RT. Base metal catalyzed dehydrogenation of ammonia–borane for chemical hydrogen storage. J Am Chem Soc 2007;129:1844–5.
[12] Stephens FH, Baker RT, Matus MH, Grant DJ, Dixon DA. Acid initiation of ammonia–borane dehydrogenation for hydrogen storage. Angew Chem Int Ed 2007;46:746–9.
[13] Bluhm ME, Bradley MG, Butterick R, Kusari U, Sneddon LG. Amineborane-based chemical hydrogen storage: enhanced ammonia borane dehydrogenation in ionic liquids. J Am Chem Soc 2006;128:7748–9.
[14] Feaver A, Sepehri S, Shamberger P, Stowe A, Autrey T, Cao G. Coherent carbon cryogel–ammonia borane nanocomposites for H_2 storage. J Phys Chem B 2007;111:7469–72.
[15] Xiong ZT, Chua YS, Wu GT, Xu WL, Chen P, Shaw W, et al. Interaction of lithium hydride and ammonia borane in THF. Chem Commun 2008;43:5595–7.
[16] Xiong ZT, Yong CK, Wu GT, Chen P, Shaw W, Karkamkar A, et al. High-capacity hydrogen storage in lithium and sodium amidoboranes. Nat Mater 2008;7:138–41.

[17] Wang P, Orimo S, Tanabe K, Fujii H. Hydrogen in mechanically milled amorphous boron. J Alloys Compd 2003;350:218–21.
[18] Wu H, Zhou W, Yildirim T. Alkali and alkaline-earth metal amidoboranes: structure, crystal chemistry, and hydrogen storage properties. J Am Chem Soc 2008;130:14834–9.
[19] Wu CZ, Wu GT, Xiong ZT, David WIF, Ryan KR, Jones MO, et al. Stepwise phase transition in the formation of lithium amidoborane. Inorg Chem 2010;49:4319–23.
[20] Luedtke AT, Autrey T. Hydrogen release studies of alkali metal amidoboranes. Inorg Chem 2010;49:3905–10.
[21] Xiong ZT, Wu GT, Chua YS, Hu JJ, He T, Xu WL, et al. Synthesis of sodium amidoborane ($NaNH_2BH_3$) for hydrogen production. Energy Environ Sci 2008;1:360–3.
[22] Spielmann J, Jansen G, Bandmann H, Harder S. Calcium amidoborane hydrogen storage materials: crystal structures of decomposition products. Angew Chem 2008;120:6386–91.
[23] Himashinie VK, Diyabalanage RPS, Semelsberger TA, Scott BL, Bowden ME, Davis BL, et al. Calcium amidotrihydroborate: a hydrogen storage material. Angew Chem Int Ed 2007;46:8995–7.
[24] Zhang Q, Tang Ch, Fang Ch, Fang F, Sun D, Ouyang L, et al. Synthesis, crystal structure, and thermal decomposition of strontium amidoborane. J Phys Chem C 2010;114:1709–14.
[25] McKee ML. Ab initio study of the formation of aminoborane from ammonia and diborane. J Phys Chem 1992;96:5380–5.
[26] Sakai S. A new mechanism of H_2BNH_2 formation in the reaction of B_2H_6 with NH_3. Chem Phys Lett 1994;217:288–92.
[27] Sakai S. Theoretical study of the chemical reactions of B_2H_6 with Lewis bases (NH_3, PH_3, H_2O, and H_2S). J Phys Chem 1995;99:9080–6.
[28] Li QS, Zhang J, Zhang S. A DFT and ab initio direct dynamics study on the hydrogen abstract reaction of $H_3BNH_3 \rightarrow H_2 + H_2BNH_2$. Chem Phys Lett 2005;404:100–6.
[29] Nguyen VS, Matus MH, Grant DJ, Nguyen MT, Dixon DA. Computational study of the release of H_2 from ammonia borane dimer $(BH_3NH_3)_2$ and its ion pair isomers. J Phys Chem A 2007;111:8844–56.
[30] Swinnen S, Nguyen VS, Nguyen MT. Potential hydrogen storage of lithium amidoboranes and derivatives. Chem Phys Lett 2010;489:148–53.
[31] Lee TB, Mckee ML. Mechanistic study of $LiNH_2BH_3$ formation from $(LiH)_4 + NH_3BH_3$ and subsequent dehydrogenation. Inorg Chem 2009;48:7564–75.
[32] Kim DY, Singh NJ, Lee HM, Kim KS. Hydrogen-release mechanisms in lithium amidoboranes. Chem Eur J 2009;15:5598–604.
[33] Shevlin SA, Kerkeni B, Guo ZX. Dehydrogenation mechanisms and thermodynamics of MNH_2BH_3 (M = Li, Na) metal amidoboranes as predicted from first principles. Phys Chem Chem Phys 2011;13:7649–59.
[34] Kim DY, Lee HM, Seo JC, Shin SK, Kim KS. Rules and trends of metal cation driven hydride-transfer mechanisms in metal amidoboranes. Phys Chem Chem Phys 2010;12:5446–53.
[35] Kohn W, Sham LJ. Self-consistent equations including exchange and correlation effects. Phys Rev 1965;140:A1133–8.
[36] Blöchl PE. Projector augmented-wave method. Phys Rev B 1994;50:17953–79.
[37] Kress G, Joubert D. From ultrasoft pseudopotentials to the projector augmented-wave method. Phys Rev B 1999;59:1758–75.
[38] Perdew JP, Wang Y. Accurate and simple analytic representation of the electron-gas correlation energy. Phys Rev B 1992;45:13244–9.
[39] Kresse G, Hafner J. Ab initio molecular dynamics for liquid metals. Phys Rev B 1993;47:558–61.
[40] Kresse G, Furthmuller J. Efficient iterative schemes for ab initio total-energy calculations using a plane-wave basis set. Phys Rev B 1996;54:11169–86.
[41] Kresse G, Furthmuller J. Efficiency of ab-initio total energy calculations for metals and semiconductors using a plane-wave basis set. Comput Mater Sci 1996;6:15–50.
[42] Perdew JP, Burke K, Ernzehof M. Generalized gradient approximation made simple. Phys Rev Lett 1996;77:3865–8.
[43] Monkhorst HJ, Pack JD. Special points for Brillouin-zone integrations. Phys Rev B 1976;13:5188–92.
[44] Henkelman G, Uberuaga BP, Jonsson H. A climbing image nudged elastic band method for finding saddle points and minimum energy paths. J Chem Phys 2000;113:9901–4.
[45] Xiong ZT, Wu GT, Hu JJ, Chen P. Ternary imides for hydrogen storage. Adv Mater 2004;16:1522–5.
[46] Henkelamn G, Arnaldsson A, Jonsson H. A fast and robust algorithm for Bader decomposition of charge density. Comput Mater Sci 2006;36:354–60.
[47] Chen XW, Yu XB. Electronic structure and initial dehydrogenation mechanism of $M(BH_4)_2 \cdot 2NH_3$ (M = Mg, Ca, and Zn): a first-principles investigation. J Phys Chem C 2012;116:11900–6.
[48] Li W, Wu GT, Chua YS, Feng YP, Chen P. Role of NH_3 in the dehydrogenation of calcium amidoborane ammoniate and magnesium amidoborane ammoniate: a first-principles study. Inorg Chem 2012;51:76–87.
[49] Zhang YS, Autrey T, Wolverton C. First-principles prediction of intermediate products in the decomposition of metal amidoboranes. J Phys Chem C 2012;116:26728–34.